

# The Attenuation of Seismic Shear Waves in Quaternary Alluvium in Santa Clara Valley, California

by James F. Gibbs, David M. Boore, William B. Joyner, and Thomas E. Fumal

**Abstract** We used shear waves, generated by an air-powered source at the ground surface and recorded in a borehole, to estimate the shear-wave quality factor at strong-motion station Gilroy no. 2. We find similar values of  $Q$  using both the decay of the spectra with depth and the slope of the spectral ratio at two depths; we find no evidence of a frequency dependence of  $Q$ . The mean value of  $Q$  over the depth range 10 to 115 m is close to 10. The use of this value over the depth of the borehole and the observed travel time of 0.358 sec gives a cumulative attenuation factor  $t^*$  of 0.036 sec for the upper 180 m of the Quaternary alluvium. This is comparable to the differential decay between Gilroy no. 2 and a rock site 1.9 km away (Gilroy no. 1), as measured from the decay of the high-frequency spectra of accelerograms from large earthquakes, plotted on a log-linear scale:  $t^* = 0.05, 0.04,$  and  $0.03$  sec for the 1979 Coyote Lake, 1984 Morgan Hill, and 1989 Loma Prieta earthquakes, respectively. The similarity between the attenuations measured from the low-strain surface source and those from the larger amplitude earthquake sources suggests that increases of damping due to nonlinear wave propagation effects are limited.

## Introduction

Many heavily developed regions of the world are in alluvial-filled valleys, and it has long been known from empirical observations that ground motions from earthquakes can be significantly altered by the near-surface geologic materials in such regions (e.g., Borchardt, 1970; Borchardt and Gibbs, 1976). Theoretical predictions of the response at specific sites need both the shear-wave velocity and attenuation as a function of depth. Such predictions are useful in analyzing the effect of site conditions on strong-ground-motion records and in estimating ground motion in future earthquakes for engineering purposes. In general, the shear-wave velocities can be more readily obtained than can the attenuation, and numerous determinations of the velocity have been reported in the literature and in engineering site studies. Although no less important than the seismic velocity, reports of shear-wave attenuation are much less common. For this reason, we report here determinations of shear-wave attenuation, as measured by the quality factor  $Q$ . (In this article we will consider shear waves only; to avoid unnecessary clutter, we do not include a subscript  $s$  to denote shear-wave velocity or attenuation.)

We first describe the experimental setup and the data collected from the active surface source. Following this, a general discussion of the model used to extract a measure of attenuation is presented. The results of applying

the model to the data are then given, using two methods to extract the attenuation.

No earthquake data were collected by the borehole instrument, but records from three large earthquakes were collected from accelerometers sited at the surface near the borehole and at a site underlain by rock 1.9 km away. The motions from these events are much larger than those from the active source used in the borehole measurements. We use these data to estimate the differential attenuation between the two accelerometer sites.

## Attenuation from a Surface Source

### Experimental Setup and Data

Gilroy no. 2 is part of a strong-motion array of six three-component accelerographs established by the U.S. Geological Survey in 1970 (and now operated by the California Strong-Motion Instrumentation Program) to study the effect of local geology on strong ground motion in earthquakes (Joyner *et al.*, 1981). The accelerograph at Gilroy no. 2 is sited on about 180 m of Quaternary alluvium. Figure 1 shows the locations of the station, a nearby rock site (Gilroy no. 1), and several earthquakes whose recordings at Gilroy stations nos. 1 and 2 will be discussed later in the article.

In a borehole located at Gilroy no. 2,  $S$  and  $P$  waves

were recorded at 2.5-m intervals to a depth of 40 m and then at every 5 m to a depth of 120 m. The overall method is essentially that described by Warrick (1974). The data were recorded on cassette tape in digital form. The measurements were made by clamping a single three-component downhole geophone in place at each depth by an electrically actuated lever arm that provided good coupling to the borehole casing. *S* waves were generated on the surface by an air-powered horizontal hammer capable of reversing the direction of the hammer blow for positive and negative polarities and of providing repeatable pulses for stacking purposes (Liu *et al.*, 1988). Stacking was done only for the bottom three traces at 110, 115, and 120 m. The shear source was placed 5 m from the center of the hole and was oriented perpendicular to a radial line from the top of the hole. With this geometry the radiation pattern is independent of the take-off angle of the rays leaving the source. The arbitrary convention "toward" and "away" was used to designate the horizontal pulse polarities. Seismograms are shown on Figure 2.

Although a reference geophone was not used, the air pressure driving the horizontal source was kept constant at 60 psi for each blow, and Liu *et al.* (1988) show that the pulses in a given direction are quite repeatable. Some compaction occurs under the source that may affect the source strength; furthermore, slight differences in source strength may occur between toward and away blows, perhaps due to lateral heterogeneities.

Initially the hole was drilled to 185 m with a nominal diameter of 8 inches (20 cm), cased with 4-inch (10-

cm) ABS sewer pipe, and backfilled (between the casing and formation) with pea gravel. The drilling was done in 1979; unfortunately, we found that the borehole was blocked at 120 m when the field work for this study was done in July of 1989. Although measurements were made approximately 10 yr after backfilling, voids may still exist between the casing and the surrounding formation, and local flexing of the casing may explain the resonances following the *S* wave at several depths (Fig. 2).

The orientation of the three-component geophone package with respect to north is unknown, because the orientation of the borehole geophone relative to the source could not be maintained (keeping one horizontal component parallel and one perpendicular to the source) when moving between depths. For analyses involving only first-arrival times and relative frequency content, we have rotated the two horizontal components into an azimuth that maximizes the integral of the squared amplitudes over a short window around the *S*-wave arrival (the traces in Figure 2 have been rotated in this way). For analyses that depend on the absolute value of the spectra, we use the square root of the sum of the squares of the amplitude spectra on the two horizontal components.

*S*-wave velocities were interpreted from the borehole data by plotting arrival times versus depth and fitting the points with straight lines (Gibbs *et al.*, 1992). The velocity model is shown in Figure 3 for the *S* waves. The approximate timing picks are shown on Figure 2 by the slant marks.

*P*-wave measurements were made at each depth by striking a steel plate with a sledge hammer (Gibbs *et al.*, 1992). The *P*-wave data were not used in this study, but they are of interest as the best indicator of water saturation. Judging from the *P*-wave velocities there is a zone of saturation, or near saturation, between depths of 8 and 15 m and below that an unsaturated zone from 15 to 22 m. From 22 m to the deepest point of the survey at 120 m the *P*-wave velocities indicate water saturation.

#### Extracting Attenuation from Downhole Measurements

In an attempt to capture the various factors that can lead to changes of spectral amplitude, we write the amplitude *A* at a depth *z* and frequency *f* as a product:

$$A(z, f) = S(z, f)C(z, f)W(z, f)G^{-1}(z) \exp(-\pi t^* f). \quad (1)$$

In this equation, *S* is a source term, *C* is a term describing the coupling of the inhole seismometer to the casing, and in turn, the casing to the surrounding material, and *W* accounts for distortions due to wave propagation (including reverberations within layers). The factor *G* accounts for geometric spreading and the change in amplitude due to variations in seismic impedance along the ray path. For vertically incident waves from a point source

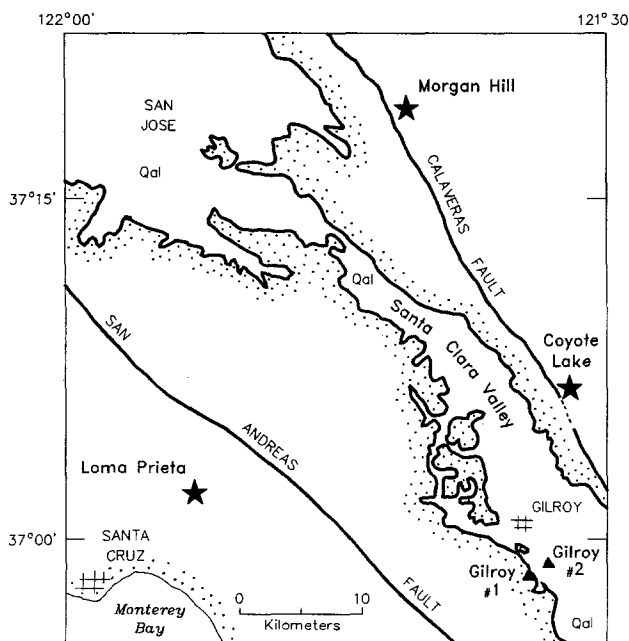


Figure 1. Map showing the locations of epicenters for three local earthquakes and the location of Gilroy strong-motion station nos. 1 and 2.

in a horizontally layered medium  $G$  is given to first order by

$$G(z) = \left( \frac{\rho(z)v(z)}{\rho(0)v(0)} \right)^{1/2} R, \quad (2)$$

where  $R$  is the effective radius for geometrical spreading, calculated from

$$R = \int_0^z \frac{v(z)}{v(0)} dz \quad (3)$$

[Newman (1973) and Aki and Richards (1980, equation (4.90) and problem 4.4)]. In equations (2) and (3),  $\rho$  is density and  $v$  is shear-wave velocity. The cumulative attenuation is described by the factor  $t^*$ . The usual parameter of interest in studies of this sort is the quality factor

$Q$ , rather than the more directly estimated attenuation coefficient  $t^*$ . The two are related by

$$t^*(z, f) = \int \frac{1}{Q} \frac{dl}{v}, \quad (4)$$

where  $v$  is the propagation velocity and the integral is taken over the path followed by the ray in traveling from the source to the receiver. At this point, most studies include justifications for the removal of the frequency dependence from all but the exponential in equation (1), and so will we.

The source term  $S$  may depend on depth for a number of reasons, including compaction of the material beneath the source (recall that only one in-hole sensor is used, and recordings at progressively shallower depths are obtained during the course of the experiment; thus, there is an inverse correlation between depth of record-

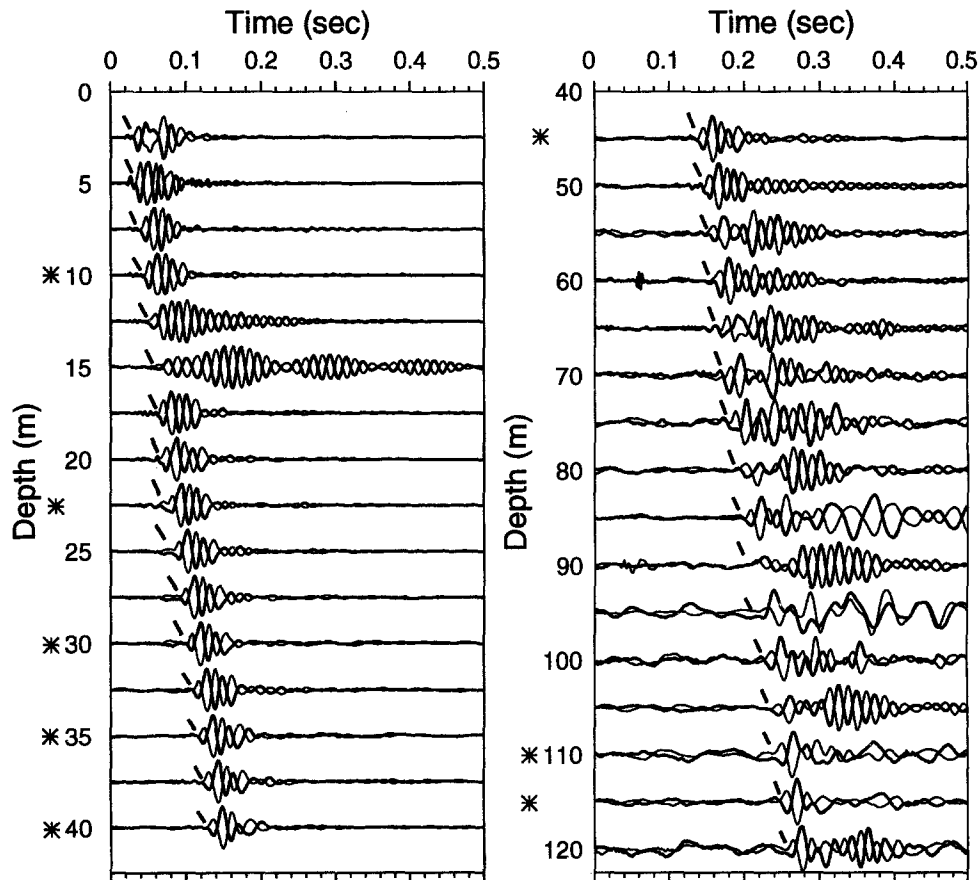


Figure 2. Shear-wave data from a borehole at Gilroy no. 2. Shear waves from positive and negative pulses of the shear source are superimposed for identification of shear arrivals. We relogged the borehole for both  $P$ - and  $S$ -wave velocities 10 years after it was drilled and assume that enough time had elapsed for the formation to tightly contact the casing. Ringing of the signals at several depths, however, suggests that some coupling problems still exist (e.g., the recordings at 12.5, 15, 90, and 105 m). Asterisks mark the traces used for  $Q$  determinations using the spectral-ratio technique.

ing and number of cycles of air-hammer blows sustained by the surface sediments). Furthermore (and probably most important), no reference recording at a fixed depth was obtained. The air pressure used to drive the horizontal hammer, however, was regulated at 60 psi for each impact. These effects are probably broadband, with the result that a ratio of the source term at two depths may be independent of frequency.

The coupling term  $C$  is probably a function of frequency. The contamination from the coupling term is most critical when spectral ratios at two depths are used to estimate the attenuation. In this case, we minimize the role of reverberation by choosing recordings at depths for which the reverberations following the initial shear wave are relatively small.

We make the initial assumption that the wave propagation term  $W$  equals unity. As discussed later, we use

synthetic seismograms to correct for deviations from this assumption.

There are two fundamentally different ways of using equation (1) to extract  $Q$ : (1) use the relative change of the spectra over a range of frequencies at two depths, and (2) use the depth decay of the absolute spectral amplitudes for a series of individual frequencies. The second method yields the frequency dependence of the attenuation directly, but it requires accurate corrections for changes in amplitude for reasons other than attenuation. The spectral ratio method does not require such corrections, as long as the non-attenuation-related amplitude changes are not a function of frequency. On the other hand, the spectral ratio method requires a model for the frequency dependence of the quality factor  $Q$ .

In the two methods discussed above for extracting the quality factor from the seismic waves, the logarithm

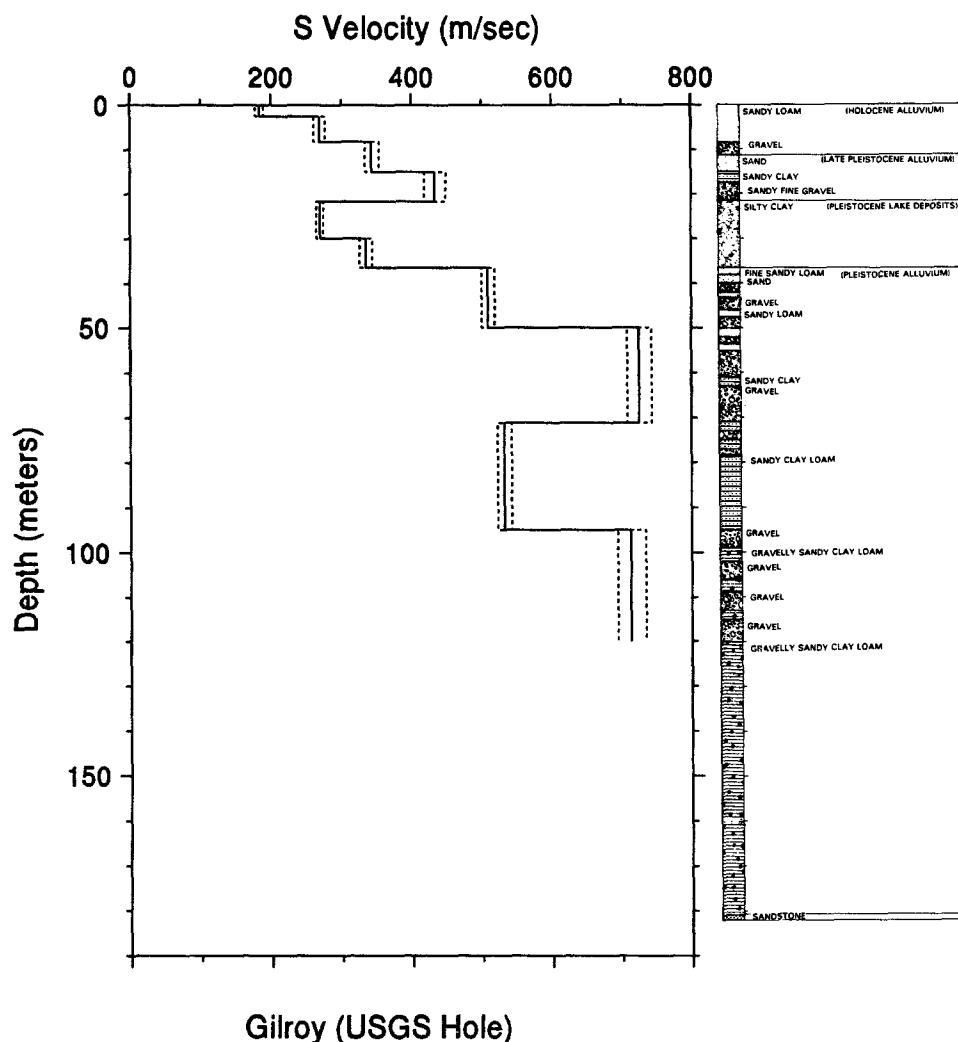


Figure 3. Velocity profile determined from  $S$ -wave picks. Dashed lines represent the upper and lower velocity limits, which are not symmetrical because they are based on the standard deviation of the slope of the least-squares line fit to the travel-time picks. Geologic log is from Joyner *et al.* (1981).

of the spectral amplitude is proportional to the inverse of the quality factor. If the spectral amplitudes have a log-normal distribution, then  $1/Q$  is a more natural variable to use than is  $Q$ . In particular, averages and statistics should be computed for  $1/Q$ . Unfortunately,  $1/Q$  is an unfamiliar quantity, and therefore in this article we will present the final results as  $Q$ , although all means and error estimates have been determined using  $1/Q$ .

In all estimates for attenuation used in this article (two methods using borehole data and one using earthquake data at closely spaced surface stations), we used synthetic seismograms to derive correction factors that account for the simplified assumptions in the initial analysis regarding wave propagation. The simulated observations were subjected to the same data processing as the observed data. Ratios between the derived attenuation and that specified in the model provided correction factors to be applied to the estimates derived from the data. As shown in the sections describing the attenuation estimates from the various methods, these corrections are generally not large. We should emphasize that the availability of independently determined shear velocities beneath the site makes this a viable approach, for we do not have to invert simultaneously for structure and attenuation.

#### Determination of $Q_i$ from Spectral Ratios

*Method.* The spectral ratio method is based on the logarithm of the ratio of the Fourier spectra at two depths,  $z_1$  and  $z_2$ . With the assumptions that  $W = C = 1$  and  $S(z_2, f) = \xi S(z_1, f)$ , equation (1) gives

$$\ln \frac{A(z_2, f)}{A(z_1, f)} = \ln \xi + \ln \frac{G(z_1)}{G(z_2)} - \pi \delta t^*(z_2, z_1, f) f, \quad (5)$$

where

$$\delta t^*(z_2, z_1, f) = t^*(z_2, f) - t^*(z_1, f). \quad (6)$$

The shape of the curve of  $\ln A(z_2, f)/A(z_1, f)$  plotted against  $f$  provides information regarding the differential  $t^*$  between the two observation depths.

Extracting  $Q$  from  $t^*$  requires assumptions regarding the frequency dependence of  $Q$ . We consider two cases:

$$Q = \left( \frac{1}{Q_i} + \frac{1}{Q_d f} \right)^{-1} \quad (7a)$$

and

$$Q = Q_r \left( \frac{f}{f_r} \right)^\eta. \quad (7b)$$

The subscripts  $i$ ,  $d$ , and  $r$  are simply used to distinguish

between the parameters, although they were chosen to represent frequency independent, frequency dependent, and reference  $Q$ , respectively.

Hough *et al.* (1988) point out that over the usual frequency range available for measurements, the form in equation (7a) can be fit to results obtained using equation (7b). The implications of both forms on extracting  $Q$  from the observations, however, is different.

If the  $Q$  dependence on frequency is given by equation (7a), then by substituting equation (7a) into equation (4) we obtain the following equation for the differential attenuation between receivers at two depths:

$$\delta t^* = \delta t_i^* + \left( \frac{f_d}{f} \right) \delta t_d^*. \quad (8)$$

In this equation,  $\delta t_i^*$  is the differential attenuation produced by substituting  $Q = Q_i$  in equation (4) for the two

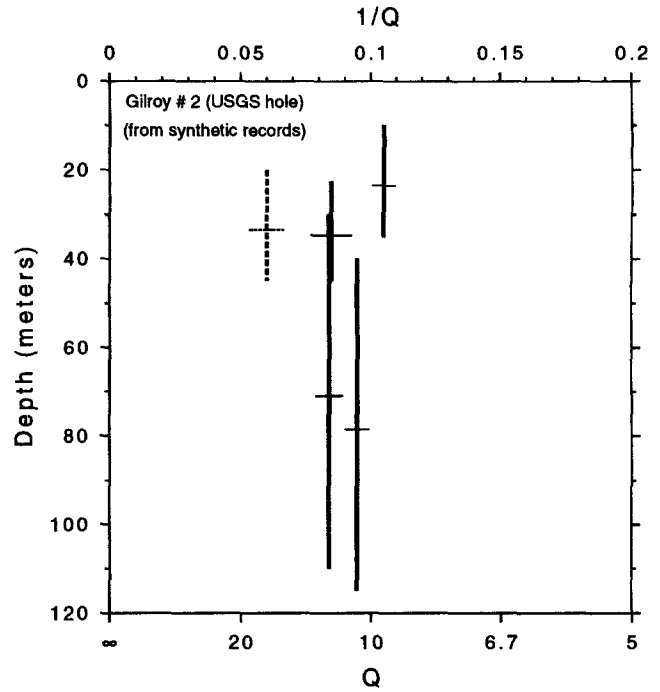


Figure 4.  $Q$  values determined by applying the spectral ratio method to synthetic seismograms computed using the borehole shear-wave velocity model at Gilroy no. 2 and an assumed frequency-independent  $Q$  value of 10 at all depths. The error range is based on the high and low estimates (68% confidence limits) of the slope from the spectral ratios. The dashed line indicates the value obtained when the upper receiver is located in the high-velocity lid at  $\sim 20$  m; values obtained from this recording seem to be severely contaminated by wave-propagation effects and are not used in the determination of  $Q$  from the data (see text).

paths leading from the source to the receivers at  $z_1$  and  $z_2$ , and correspondingly for  $\delta t_d^*$ , with  $Q = Q_d$ . Substituting equation (8) into equation (5),

$$\ln \frac{A(z_2, f)}{A(z_1, f)} = \ln \xi + \ln \frac{G(z_1)}{G(z_2)} - \pi \delta t_d^* f_d - \pi \delta t_i^* f. \quad (9)$$

If this model is correct, a plot of the ratio of  $\ln A$  versus  $f$  can be fit by a straight line from whose slope  $Q_i$ , the frequency-independent part of the quality factor, can be extracted. Assuming that  $Q_i$  is independent of depth, the slope  $s$  is related to the quality factor by

$$Q_i = -\pi \delta \tau / s, \quad (10)$$

where  $\delta \tau$  is the differential travel time for waves traveling from the source to the two depths  $z_1$  and  $z_2$ . The component  $Q_d$  can be recovered from the zero-frequency intercept of the straight line fit to the spectrum if corrections are made for the geometrical spreading factor and for the source factor.

If  $Q$  is proportional to a power of frequency as in

equation (7b), then by substituting equation (7b) into equation (4) we obtain

$$\delta t^* = \left( \frac{f_r}{f} \right)^\eta \delta t_r^* \quad (11)$$

and

$$\ln \frac{A(z_2, f)}{A(z_1, f)} = \ln \xi + \ln \frac{G(z_1)}{G(z_2)} - \pi \delta t_r^* \left( \frac{f_r}{f} \right)^\eta f. \quad (12)$$

With this model for  $Q$ , the slope of  $\ln A$  versus  $f$  is not linear.  $Q_r$  and  $\eta$  can be obtained by model fitting the spectral ratio at pairs of depths or by fitting the depth dependence of the spectra for separate frequency bands.

*Correction Factors.* We generated synthetic seismograms using a computer program written by Robert B. Herrmann (HSPEC91). This is a complete wave-propagation program that uses wavenumber integration and a layered earth model; the calculations include near-field terms and all inter-bed reflections. Synthetic seismograms were generated for the depths at which the data were recorded, using the shear-wave velocity model at Gilroy no. 2 (Fig. 3), a  $Q$  of 10, and a horizontal trans-

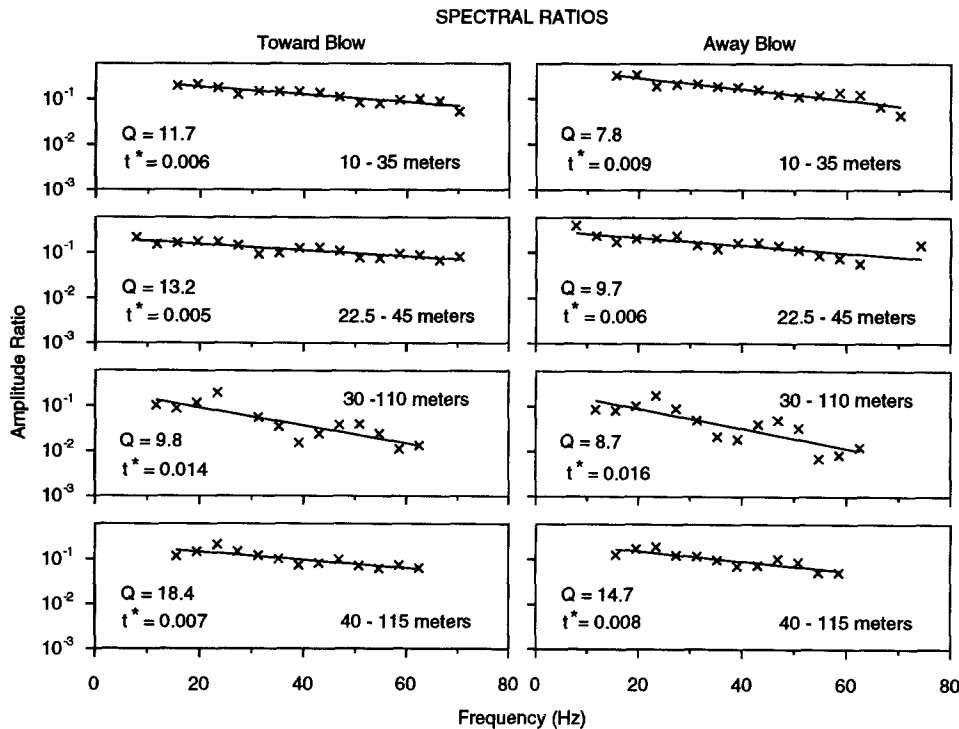


Figure 5. Spectral ratios from observations, for the depth intervals shown, with least-squares fit over the indicated frequency bands. The  $Q$  and  $t^*$  values determined from the slopes are shown for the "toward" and "away" direction of the shear-wave hammer.

verse source at the surface. The spectral ratio method, equation (9), was used on the synthetic seismograms to obtain the  $Q_i$  values shown in Figure 4 (using a frequency band given by a signal-to-noise analysis of the data). There is close agreement with the input value of 10, indicating that overall the assumptions used in deriving equation (9) are justified. There are some systematic differences, however. For a given depth range we use the ratio of the derived  $Q$  to the input value of 10 as a correction to apply to the  $Q_i$  extracted from the data. The  $Q$  given by the dashed value in Figure 4, for the depth range of 20 to 45 m, is anomalously high. Calculations using synthetics for nearby depths demonstrate

that the anomalous  $Q$  is associated with the receiver at 20 m, within a high-velocity lid overlying a low-velocity region of lake-bed sediments. The effect is due to an interference phenomenon that is not easily seen in the time-series, yet is readily apparent in both the synthetic and the observed spectra (the data yield a negative  $Q$ ): the spectra at 20 m, relative to the spectra at 17.5 and 22.5 m, is deficient in the higher frequencies (30 to 70 Hz), thus skewing the slope of the spectral ratio toward positive values and giving anomalously high  $Q$  estimates. Using the next deeper receiver, at 22.5 m, eliminates the problem. Based on the results from the synthetic seismograms, we have ignored the 20-m recording in the  $Q$  derived from the spectral ratio method.

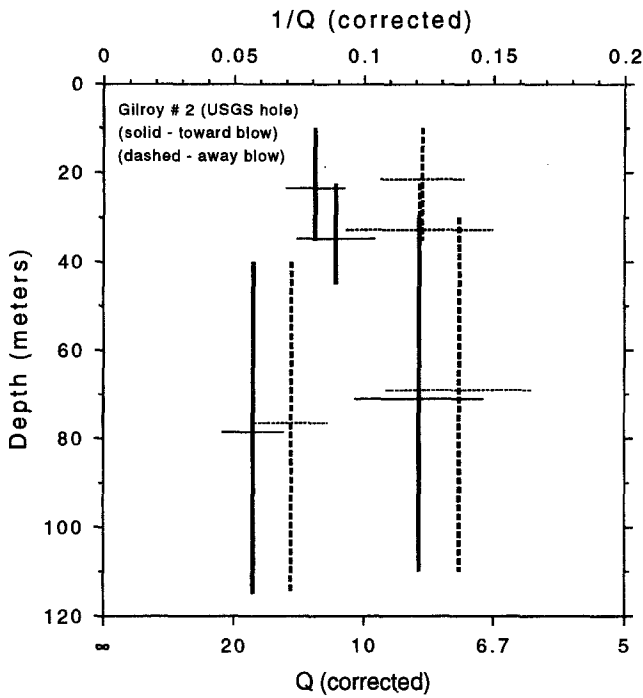


Figure 6. Frequency-independent component of the near-surface shear-wave attenuation  $Q_i$  from borehole data. Horizontal bars indicate the error range and the vertical bars the depth range. The error range is based on the high and low estimates (68% confidence limits) of the slope from the spectral ratios.

Table 1  
Shear-Wave  $Q$

Depth interval, m	Shear $1/Q$ (avg. horiz. blows)	Correction factor	Corrected $1/Q$
10-35	0.107	0.953	0.102
22.5-45	0.089	1.180	0.105
30-110	0.108	1.192	0.129
40-115	0.061	1.057	0.065
Mean shear-wave $1/Q$ and standard deviation			0.100 ± 0.026

(The 68% confidence limits on the mean of  $1/Q$  are 0.084 to 0.116.)

**Results.** For a spectral ratio method to be successful the data must have a good signal-to-noise ratio. From Figure 2 we chose traces at depths of 10, 22.5, 35, 40, 45, 110, and 115 m that appeared to have a simple  $S$ -wave arrival, free of ringing (well coupled), lower noise, and the coda relatively free of interfering secondary arrivals. The time window used for the spectral computations was

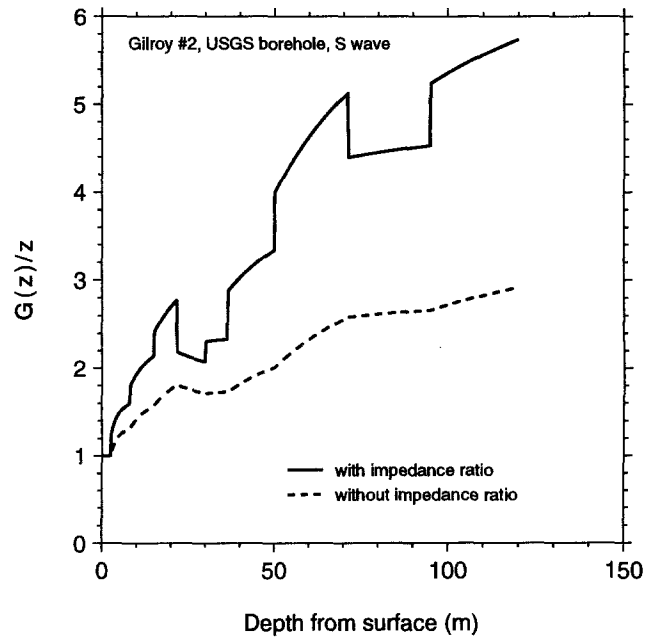


Figure 7. Computed geometrical spreading and impedance correction. The dashed line shows the effective radius ( $R$ ) alone, as computed from equation (3), and the solid line shows the combination of both the impedance correction and geometrical spreading [equation (2)]. To emphasize the difference between these corrections and the assumption of simple inverse-distance geometrical spreading with no corrections for amplitude changes produced by changes in seismic impedance, the factors computed from equations (2) and (3) have been normalized by the distance from the source to the receiver.

started approximately 20 msec before the *S*-wave arrival and has a total length of 150 msec. The resulting spectra are defined at 128 positive frequencies with a frequency spacing just under 4 Hz (Mueller, 1990). The spectral window has a cosine taper of 10% at both ends. Spectral ratios are fit with a least-squares line in the frequency interval where the signal-to-noise ratios are >2. Because the *S*-wave arrival times are <150 msec for depths <45 m, the noise sample for the spectra (for determining signal-to-noise ratios) was taken from the coda at 850 to 1000 msec. Although this may introduce minuscule amounts of signal, the end result when the signal-to-noise ratio is computed is merely to reduce slightly the range of frequencies over which the slope is computed. The same frequency interval is used for opposite horizontal blows recorded at the same depth and for the analysis of the synthetic seismograms. The spectra and the regression fits are shown in Figure 5. Initially we estimated *Q* for seven depth intervals (Gibbs, 1992). We based our final results on the four depth intervals for which the receiver depths are different, so that the determination of *Q* represents independent measurements. The results are shown in Figure 6 and are tabulated in Table 1. Implicit in these results is the assumption that *Q* does not have the frequency dependence given by equation (7b).

The linearity of the spectral-ratios (e.g., Fig. 5) supports the assumption over the frequency ranges used to fit the data. We also note that there is no indication that *Q* varies with depth over the range of measurements.

#### Determination of *Q* from Depth Decay

*Method.* Although we can weakly rule out the *Q* model in equation (7b), the spectral ratio technique tells us nothing about the frequency-dependent component *Q<sub>d</sub>* if the model given by equation (7a) applies. To check for this type of frequency dependence, we have determined *Q* from the depth dependence of spectral values at individual frequencies, after correcting for impedance changes and geometrical spreading. The analysis is similar to that in the spectral ratio method, with the assumption that there is no depth dependence either to the source ( $\xi = 1$ ) or to the quality factor *Q*. By working with one frequency at a time, we can solve for *Q* directly. We also recognize that the fundamental independent parameter is travel time  $\tau$  between the source and the receiver, and not the depth *z*; we use the observed mapping between  $\tau$  and *z* to eliminate *z*. From the previous equations we find

$$G(\tau)A(\tau, f) \propto \exp \left[ -\pi \left( \frac{f}{Q} \right) \tau \right], \quad (13)$$

and the slope of  $\ln G(\tau)A(\tau, f)$  versus observed time  $\tau$  provides an estimate of *Q* at frequency *f*.

*Correction Factors.* Extracting *Q* from the depth decay, equation (13), requires a correction for geometrical spreading, *G*( $\tau$ ) and for the first-order effect of the changing seismic impedances on the wave amplitudes. These corrections are shown in Figure 7 normalized to the inverse of the source-receiver distance. Clearly, the effect of the depth-dependent velocities produces a major effect on the amplitude of the waves in the absence of any damping. The geometrical spreading has been computed assuming both a source directly over the borehole (0-m offset), the formula for which is very simple [equation (3)], and a source offset of 5 m, as in the experiment [Aki and Richards, 1980, equation (4.90) and Problem 4.4]. The difference in the two results is important only for the recordings at the shallowest depths, for which the difference between a point source and the actual 2.3-m extended source is probably more important.

Because of their size and their origin (ray theory), we viewed the large corrections shown in Figure 7 with some skepticism. We allayed our skepticism by subjecting the spectra from the synthetic seismograms to these corrections [as in equation (13)] and found that the derived *Q* was very close to the input value of 10 (Fig. 8) and showed a slight frequency dependence. The ratios

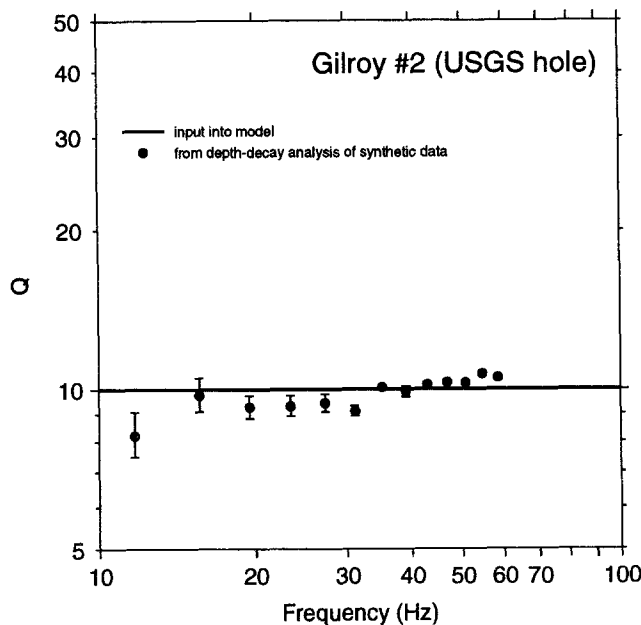


Figure 8. *Q* from depth decay of spectra from synthetic seismograms, as a function of frequency. The Gilroy no. 2 velocity model and a *Q* value of 10 are used in the synthetic computation. The bars indicate the standard deviation of the *Q* values. The analysis shows a slight frequency dependence, even though a frequency-independent *Q* was specified in the model. We presume that the same bias exists in the real data, and we remove it by applying correction factors determined from the results shown in this figure.

of the derived values of  $Q$  to the input value 10 were used as correction factors at each frequency for the  $Q$  values obtained from the observed data.

*Results.* The spectra were computed for a 150 msec window starting approximately 20 msec before the first  $S$  arrival and corrected for the factor  $G$ , as in equation (13). The travel-time (and thus depth) dependence is shown in Figure 9, along with the fits of straight lines to the data [although shown for all travel times, the fits were to the points at depths greater than 7.5 m (a travel time of 0.038 sec) and excluded the obvious outlying points for 15 m (a travel time of 0.058 sec)]. The values of  $Q$  extracted from the decay of the spectra are shown in Figure 10, which also shows the attenuation determined from the spectral ratio method. There is signifi-

cant overlap of the 68% confidence limits of the  $Q$  estimate from the spectral ratio method and the plus and minus one standard deviation bars from the spectral decay method, indicating that there is very little, if any, frequency dependence to the derived  $Q$ .

### Attenuation from Local Earthquake Data

Another source of information regarding the attenuation in the vicinity of Gilroy no. 2 are recordings of earthquakes on the earth's surface at Gilroy station nos. 1 and 2 (no earthquakes were recorded downhole). We estimate the differential attenuation between these stations using data from the 1979 Coyote Lake, 1984 Morgan Hill, and 1989 Loma Prieta earthquakes recorded by strong-motion accelerographs at those stations (Con-

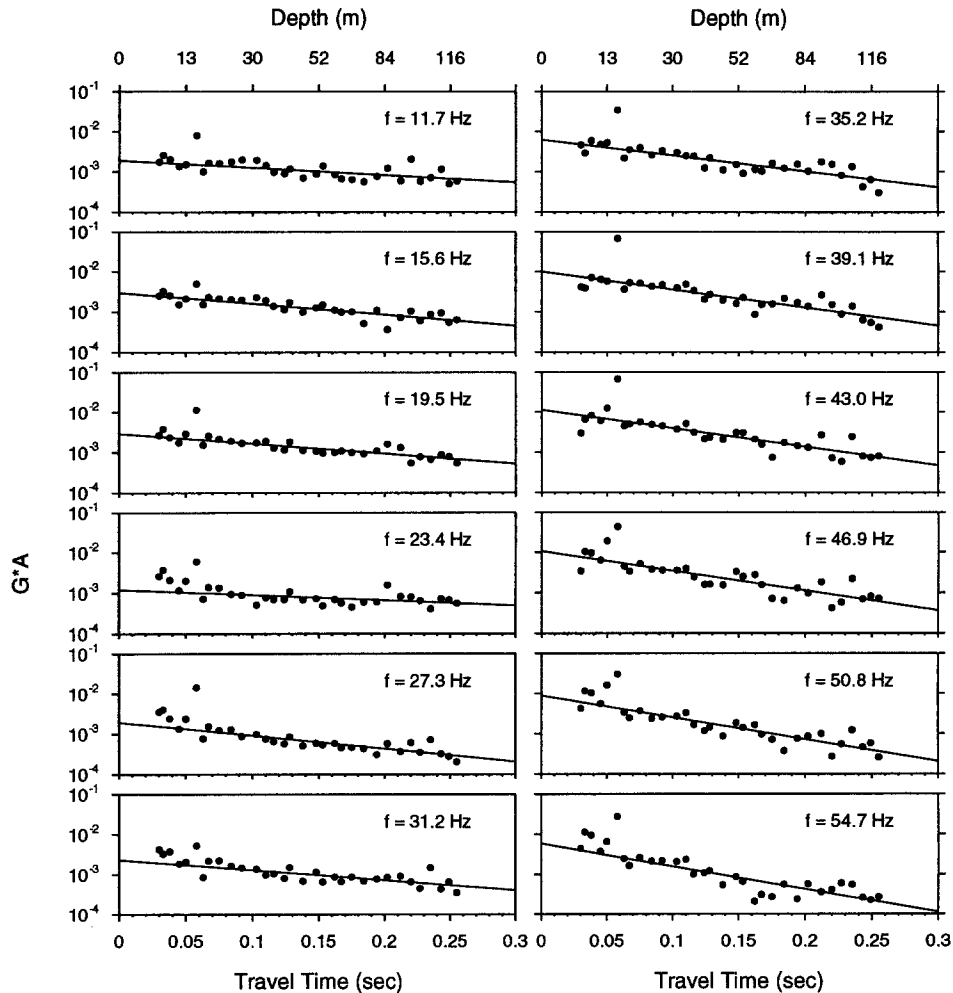


Figure 9. Spectral amplitude corrected for geometrical spreading and seismic impedance as a function of source-to-receiver travel time, from data produced by "toward" hits; the depths corresponding to the travel times are shown at the top, rounded to whole units. Each plot is for the single frequency shown [the plot for the highest frequency (58.6 Hz) is not shown, but it has the same character as the others]. The slopes are used to calculate the  $Q$ 's shown by the squares and open circles in Figure 10.

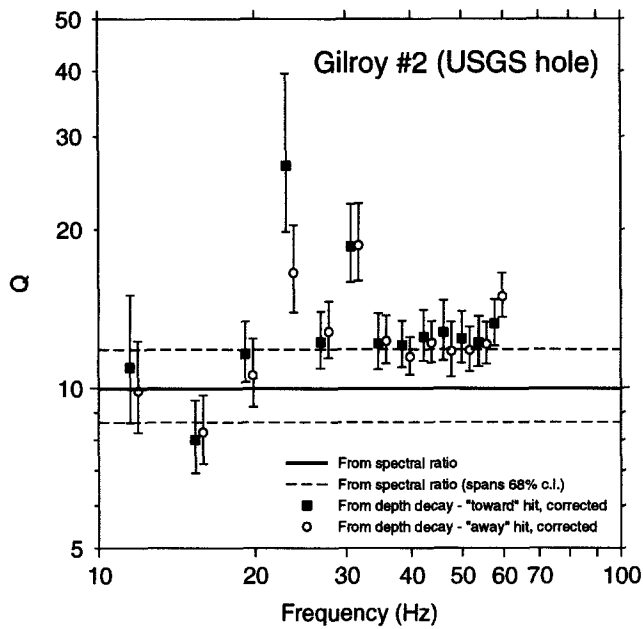


Figure 10. Shear-wave  $Q$  determined from spectral ratios (Table 1) and from depth decay of corrected amplitude spectra as a function of frequency. The dashed lines span the 68% confidence limits of the  $Q$  value from the spectral ratio method, and the bars indicate  $\pm 1$  SD of the  $Q$  estimates from the spectral decay. These error estimates include contributions from both the uncertainties in the uncorrected estimates and the uncertainties in the correction factors obtained from the simulated motions.

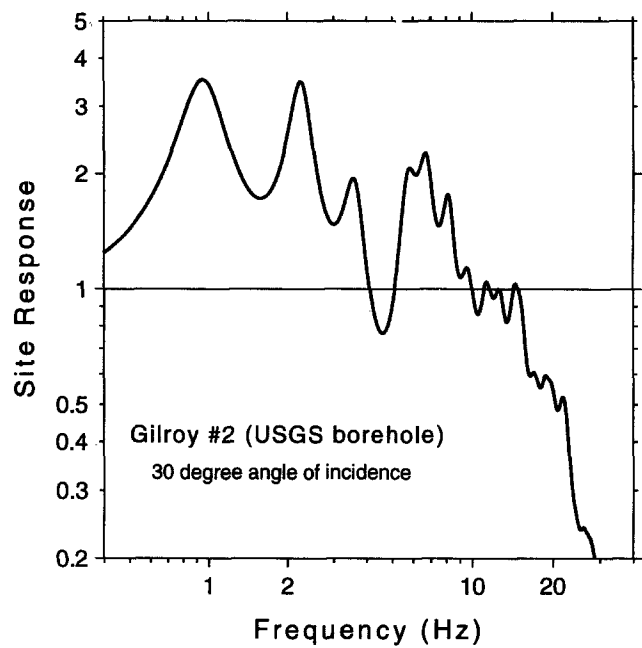


Figure 11. Site response for  $SH$  waves at  $30^\circ$  incidence beneath Gilroy no. 2. This calculation used a constant  $Q$  of 12 in the sediments, whereas a  $Q$  of 10 was used in the calculations from which correction factors for  $\kappa$  were derived.

verse, 1984). [Aftershocks of the Loma Prieta earthquake have been recorded at these stations by instruments installed after the mainshock (Darragh and Shakal, 1991); we have not used these data.] The earthquakes range in magnitude from 5.8 to 6.9 (Table 2), and their motions have larger amplitudes and generally lower frequencies than do the motions from the shear-wave source. For each earthquake, the data have been rotated into directions radial and transverse with respect to the epicenter.

*Method.* Anderson and Hough (1984) hypothesize that the fall-off of the high-frequency acceleration spectrum can be approximated by,

$$A(f) = A_0 e^{-\pi \kappa f} \quad f > f_E \quad (14)$$

where  $A$  is the amplitude,  $\kappa$  is the spectral decay parameter, and  $f_E$  is defined as the "frequency above which the spectral shape is indistinguishable from exponential decay." By taking the difference in  $\kappa$  for a single earthquake at both stations, we hope to isolate that part of the attenuation due to propagation through the sediments underlying Gilroy no. 2. We assume that the attenuation along the path from the source to the base of the alluvium at Gilroy no. 2 is the same as the attenuation along the path from the source to the surface at Gilroy no. 1

Table 2  
Spectral Decay Parameters and Earthquake Data

Earthquake	Year	Magnitude (M)	Distance, km	Max. hor., acc. g	$\kappa$ (avg.) rad. & transv.	$\kappa$ (diff.) $\kappa_{Qa1} - \kappa_{Rock}$	Correction factor	$\kappa$ (diff.) Corrected
Gilroy no. 2								
Coyote Lake	1979	5.8	14.2	0.25	0.058	0.036	1.32	0.048
Morgan Hill	1984	6.2	38.8	0.21	0.065	0.034	1.20	0.041
Loma Prieta	1989	6.9	29.9	0.37	0.080	0.022	1.28	0.028
Gilroy no. 1								
Coyote Lake			15.9	0.12	0.022			
Morgan Hill			39.4	0.10	0.031			
Loma Prieta			28.6	0.48	0.058			

(the stations are separated by 1.9 km). With this assumption in mind, the difference in  $\kappa$  from the two Gilroy stations can be compared to the  $Q$  results obtained from the borehole observations.

**Correction Factors.** The variations in velocity beneath Gilroy no. 2 will produce significant distortions in the spectral shape (Fig. 11), and it is important to account for the effect of these distortions on the computed  $\kappa$ . As we did in the analysis of the borehole data, we derive correction factors by comparing  $\kappa$  derived from simulated data with the value computed for the model used in the simulations. We simulated the effect of the alluvial section at Gilroy no. 2 by using C. Mueller's im-

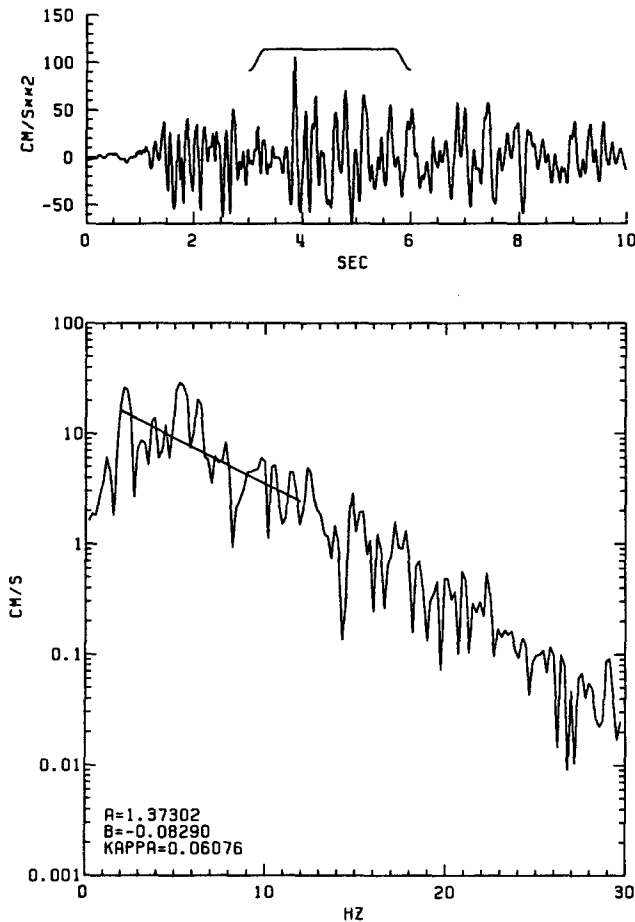


Figure 12. Synthetic seismogram through the alluvial section at Gilroy no. 2. The input at the base of the alluvium used to produce this seismogram was the radial component of the Morgan Hill earthquake record at Gilroy no. 1; six such analyses were performed (two components for three earthquakes). The two differential  $\kappa$  values for each earthquake (one for each horizontal component) were averaged and used to compute correction factors; these factors were used to correct the observed differential  $\kappa$ 's for spectral distortions produced by the sediments underlying Gilroy no. 2.

plementation (program RATTLE) of the Haskell plane-wave layer-matrix wave propagation formulation (Haskell, 1960) to generate a synthetic seismogram using the borehole velocity model, a  $Q$  of 10, and an angle of incidence of  $30^\circ$ . The surface recordings from the three earthquakes at the rock site (Gilroy no. 1) were used as input at the base of the alluvium. The synthetic seismograms were analyzed in the same manner as the earthquake data for  $\kappa$  (Fig. 12), and the difference between Gilroy nos. 1 and 2 was computed. The analysis was repeated for both horizontal components of each earthquake as input, and correction factors were determined that converted the  $\kappa$  differences to the values corresponding to the assumed  $Q$ . These correction factors, which range from 1.20 to 1.32 (Table 2), were applied to the differential  $\kappa$  obtained from the data.

**Results.** Figure 13 shows the windowed time series and Figure 14 the  $\kappa$  slopes. The resulting values of  $\kappa$  are shown in Table 2. The values were obtained by fitting a least-squares line over the frequency range of 2 to 12 Hz (with one exception—a range of 4 to 12 Hz was used for the radial component from the Coyote Lake earthquake recorded at Gilroy no. 1; see Fig. 14). The 2- to 12-Hz frequency band covers the upper end of the frequency interval of usual interest to structural engineers. Trials using different frequency ranges indicate that the  $\kappa$  values have an uncertainty of at least  $\pm 0.005$  sec.

For comparison with the differential attenuation obtained from the earthquake data, the  $t^*$  through the alluvium section was calculated from

$$t^* = \frac{t}{Q}, \quad (15)$$

where  $t$  = the total shear-wave travel time (0.358 sec) through the 180-m alluvial section at Gilroy no. 2 [the total travel time to bedrock was obtained from a previous logging (Joyner *et al.*, 1981)]. This gives a computed value of  $t^*$  through the alluvial section of  $0.036 \pm 0.008$  sec.

The differences in  $\kappa$  values between the value on alluvium at Gilroy no. 2 and the value on rock at Gilroy no. 1 are shown in Table 2. These  $\kappa$  differences are within a factor of 1.4 of the value computed from the small-amplitude borehole data for Gilroy no. 2 (0.036 sec). These observations suggest that the amount of increase in damping associated with increases in earthquake accelerations is limited. The observations, however, apply to the total damping over the 180-m alluvial section and do not preclude significant nonlinear behavior within individual layers, as shown by Chin and Aki (1993), who modeled the response of Gilroy no. 2 in the Loma Prieta earthquake.

We infer that the amount of increase in damping due to nonlinearity is limited. That inference is based on the presumption that increases in damping will be reflected in larger values of  $\kappa$ . We are aware that Yu *et al.* (1993) have done simulations showing that nonlinear effects can produce a decrease in  $\kappa$  over a certain range of frequency for larger motions.

### Summary and Discussion

We have determined shear  $Q$  *in situ* from borehole measurements in Quaternary alluvium. We determined the attenuation values using both the spectral ratio of motions at two depths and the depth decay of spectral ordinates at individual frequencies. (Another method for determining attenuation uses changes in the rise time of the initial wave arrival; we did not use the rise-time method because it is more subject to errors both from  $P$ -wave contamination and from reflection and scatter-

ing in heterogeneous material.) The spectral-ratio method has the advantage of not requiring corrections for amplitude changes produced by geometrical spreading and variations in seismic impedance. The spectral ratio method has the disadvantage that it determines only the frequency-independent component of  $Q$ . The depth-decay method directly yields any frequency dependence of  $Q$ , but by using absolute amplitudes requires more assumptions than does the spectral-ratio method. We check both methods by using synthetic seismograms computed for the shear-wave velocity model from the borehole at Gilroy no. 2, subjecting the synthetic data to the same processing and methods as the downhole data to recover the assumed value of  $Q$ . The results indicated that the layering of the sediments as represented by our shear-wave velocity model has a small influence in the computed  $Q$ ; the ratios were used to correct the  $Q$  values determined from the real data. Both methods give consistent results and a value of  $Q$  near 10 for the upper 115 m of Quaternary alluvium in Santa Clara Valley near

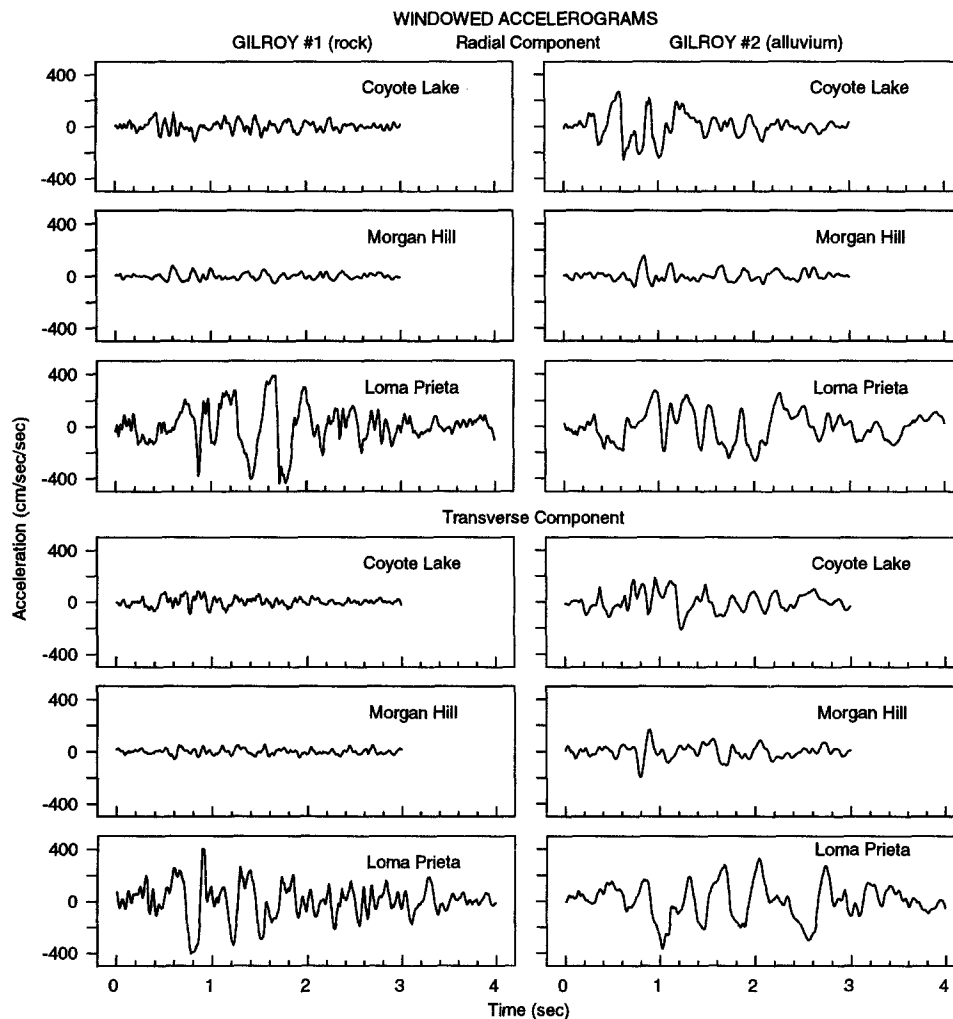


Figure 13. Portions of horizontal-component accelerograms of three local earthquakes recorded at Gilroy nos. 1 and 2 containing the  $S$  wave.

Gilroy, California, with no evidence for a frequency-dependent  $Q$ .

After the Loma Prieta earthquake additional holes were drilled near Gilroy no. 2. Shear  $Q$  was measured by K. H. Stokoe II and M. N. Toksöz using cross-hole data and by Agabian and Associates and M. N. Toksöz using downhole data. The results are given in EPRI (1993). Most of the cross-hole measurements were made at much higher frequencies than ours. Those measurements made in our frequency range gave significantly higher values of shear  $Q$  than we obtained. The downhole measurements were made at only five depths, and some of the data were noisy. The shear- $Q$  values obtained from the downhole data were generally similar to the values we obtained.

Near-surface values of shear  $Q$  similar to those we

report here have been observed by others at a number of different localities using various methods (e.g., McDonald *et al.*, 1958; Kudo and Shima, 1970; Newman and Worthington, 1982; Meissner and Theilen, 1983; Boatwright *et al.*, 1986; Malin *et al.*, 1988; Gibbs and Roth, 1989; Fletcher *et al.*, 1990; Jongmans, 1990). Most of these studies find low  $Q$  values (in the range 2 to 20 at frequencies  $<100$  Hz) in borehole depths to 500 m.

Differential  $\kappa$  (corrected for layering effects) values from three large earthquakes recorded at Gilroy nos. 2 and 1 (rock site 1.9 km from Gilroy no. 2) are within a factor of 1.4 of the  $t^*$  values through the alluvial section at Gilroy no. 2 determined from borehole measurements. This agreement implies that the higher frequency data from borehole measurements is applicable to the lower frequency band of engineering interest. The similarity

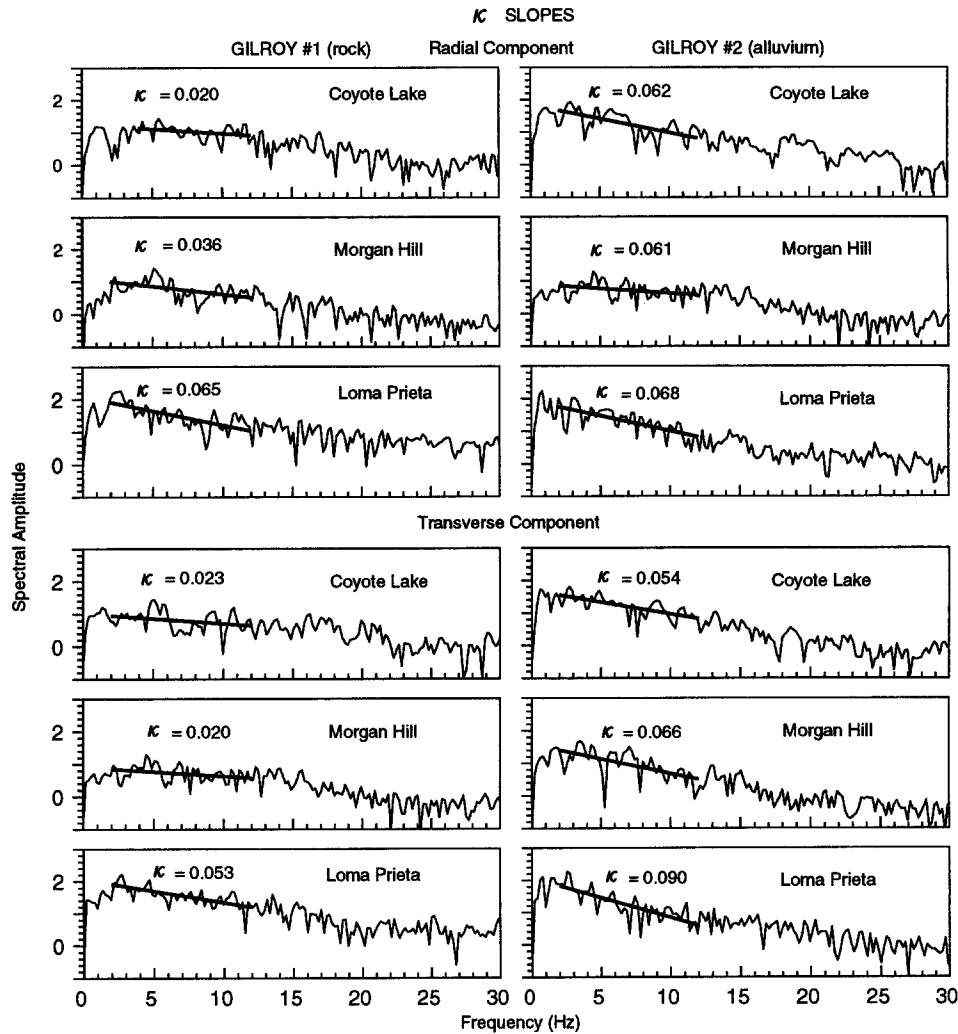


Figure 14.  $\kappa$  slopes from the spectra of windowed-accelerograms of Figure 13. The average (radial and transverse) slope values are shown in Table 2. All spectra are fit between 2 and 12 Hz except the recording of the Coyote Lake earthquake at Gilroy no. 1; the spectrum from this record was fit between 4 and 12 Hz because of the spectral hole near 2 Hz. The  $\kappa$  values shown for Gilroy no. 2 have not been corrected for the effects of layering.

between the attenuation measured from the low-strain surface source and those from the larger amplitude earthquake sources suggests that increases of damping due to nonlinear wave propagation effects may be limited.

The  $Q$  measured here may include some contribution from scattering as well as anelastic attenuation. Scattering may be due in part to layering at a scale finer than represented by our velocity survey. We believe it appropriate to include the effects of such scattering in a  $Q$  estimate intended for use in predicting ground motions, because data will not usually be available to model the effect of the finer layering.

If the attenuation we measure is entirely due to anelastic attenuation, it would produce approximately  $100 \times 1/\pi Q \ln 10 = 7\%$  decrease in seismic velocity for each decade decrease in frequency (Aki and Richards, 1980, equation 5.77). To the extent that attenuation is due to scattering, the effect would be less (Richards and Menke, 1983). Most velocity logging is done at frequencies of 20 to 60 Hz, and because of the possible dependence of velocity on frequency, caution should be used in applying these measurements of velocity to earthquake-produced seismic waves, whose frequencies are principally between 0 and 10 Hz.

### Acknowledgments

We thank Charles Mueller and Robert B. Herrmann for their computer programs, Robert E. Westerlund for his help in the field (in 100°F heat), and Hsi-Ping Liu and Robert E. Westerlund for designing and building the shear-wave hammer. Discussions with participants at several workshops sponsored by the Electric Power Research Institute and organized by John Schneider were useful. In addition, we are grateful to Sue Hough, Hsi-Ping Liu, Kei Aki, John G. Anderson, and an anonymous reviewer for comments on the manuscript. This work was partially funded by the U.S. Nuclear Regulatory Commission.

### References

- Aki, K. and P. G. Richards (1980). *Quantitative Seismology: Theory and Methods*, 2 vols., W. H. Freeman and Co., San Francisco, Calif.
- Anderson, J. G. and S. E. Hough (1984). A model for the shape of the Fourier amplitude spectrum of acceleration at high frequencies, *Bull. Seism. Soc. Am.* **74**, 1969–1993.
- Boatwright, J., R. Porcella, T. Fumal, and H.-P. Liu (1986). Direct estimates of shear wave amplification and attenuation from a borehole near Coalinga, California, *Earthquake Notes* **57**, 8.
- Borcherdt, R. D. (1970). Effects of local geology on ground motion near San Francisco Bay, *Bull. Seism. Soc. Am.* **60**, 29–61.
- Borcherdt, R. D. and J. F. Gibbs (1976). Effects of local geologic conditions in the San Francisco Bay region on ground motions and intensities of the 1906 earthquake, *Bull. Seism. Soc. Am.* **66**, 467–500.
- Chin, B.-H. and K. Aki (1993). Non-linear site response study during the 1989 Loma Prieta earthquake, *Bull. Seism. Soc. Am.* **83** (in press).
- Converse, A. (1984). AGRAM: A series of computer programs for processing digitized strong-motion accelerograms, *U.S. Geol. Surv. Open-File Rept.* 84-525.
- Darragh, R. B. and A. F. Shakal (1991). The site response of two rock and soil station pairs to strong and weak ground motion, *Bull. Seism. Soc. Am.* **81**, 1885–1899.
- EPRI (1993). Guidelines for determining design basis ground motions, *EPRI Report TR-102293*, Electric Power Research Institute, Palo Alto, Calif.
- Fletcher, J. B., T. Fumal, H.-P. Liu, and L. C. Carroll (1990). Near-surface velocities and attenuation at two boreholes near Anza, California, from logging data, *Bull. Seism. Soc. Am.* **80**, 807–831.
- Fumal, T. E., J. F. Gibbs, and E. F. Roth (1982). In-situ measurements of seismic velocity at 10 strong motion accelerograph stations in Central California, *U.S. Geol. Surv. Open-File Rept.* 82-407.
- Gibbs, J. F. and E. F. Roth (1989). Seismic velocities and attenuation from borehole measurements near the Parkfield prediction zone, central California, *Earthquake Spectra* **5**, 513–537.
- Gibbs, J. F. (1992). The attenuation of seismic shear waves in Quaternary alluvium from borehole measurements and local earthquakes, Santa Clara Valley, California, *Seism. Res. Lett.* **63**, 1.
- Gibbs, J. F., T. E. Fumal, D. M. Boore, and W. B. Joyner (1992). Seismic velocities and geologic logs from borehole measurements at seven strong-motion stations that recorded the Loma Prieta earthquake, *U.S. Geol. Surv. Open-File Rept.* 92-287.
- Haskell, N. A. (1960). Crustal reflection of plane SH waves, *J. Geophys. Res.* **65**, 4147–4150.
- Hough, S. E., J. G. Anderson, J. Brune, F. Vernon III, J. Berger, J. Fletcher, L. Haar, T. Hanks, and L. Baker (1988). Attenuation near Anza, California, *Bull. Seism. Soc. Am.* **78**, 672–691.
- Jongmans, D. (1990). In-situ attenuation measurements in soils, *Eng. Geol.* **29**, 99–118.
- Joyner, W. B., R. E. Warrick, and T. E. Fumal (1981). The effect of Quaternary alluvium on strong ground motion in the Coyote Lake, California, earthquake of 1979, *Bull. Seism. Soc. Am.* **71**, 1333–1349.
- Kudo, K. and E. Shima (1970). Attenuation of shear waves in soil, *Earthquake Res. Inst.* **48**, 145–158.
- Liu, H.-P., R. E. Warrick, R. E. Westerlund, J. B. Fletcher, and G. L. Maxwell (1988). An air-powered impulsive shear-wave source with repeatable signals, *Bull. Seism. Soc. Am.* **78**, 355–369.
- Malin, P. E., J. A. Waller, R. D. Borcherdt, E. Cranswick, E. G. Jensen, and J. VanSchaack (1988). Vertical seismic profiling of Oroville microearthquakes: Velocity spectra and particle motion as a function of depth, *Bull. Seism. Soc. Am.* **78**, 401–420.
- McDonal, F. J., F. A. Angona, R. L. Mills, R. L. Sengbush, R. G. Van Nostrand, and J. E. White (1958). Attenuation of shear and compressional waves in Pierre Shale, *Geophysics* **23**, 421–439.
- Meissner, R. and F. Theilen (1983). Attenuation of seismic waves in sediments, in *Proceeding of the Eleventh World Petroleum Congress*, London, John Wiley & Sons Limited, vol. 2, 363–379.
- Mueller, C. S. (1990). Computer programs for analyzing digital seismic data, *U.S. Geol. Surv. Open-File Rept.* 90-35.
- Newman, P. (1973). Divergence effects in a layered earth, *Geophysics* **38**, 481–488.
- Newman, P. J. and M. H. Worthington (1982). In-situ investigation of seismic body wave attenuation in heterogeneous media, *Geophys. Prospect.* **30**, 377–400.
- Richards, P. G. and W. Menke (1983). The apparent attenuation of a scattering medium, *Bull. Seism. Soc. Am.* **73**, 1005–1021.

- Warrick, R. E. (1974). Seismic investigation of a San Francisco Bay mud site, *Bull. Seism. Soc. Am.* **64**, 375–385.
- Yu, G., J. G. Anderson, and R. Siddharthan (1993). On the characteristics of nonlinear soil response, *Bull. Seism. Soc. Am.* **83**, 218–244.

U.S. Geological Survey  
345 Middlefield Road  
Menlo Park, California 94025

Manuscript received 7 January 1993.